A Novel optimization strategy for improving microgrid with PV/Wind based AC/DC microgrid system

Priyanka Mishra[*1], Jagdish B Helonde[2], Prakash G Burade[3]

[1]Research scholar, Department of Electrical and Electronic Engineering, Sandip University, Mahiravani, Nashik, 422213, India, Email: poojamishra1112@gmail.com
[2]Professor, Department of Electrical and Electronic Engineering, Sandip University, Mahiravani, Nashik, 422213, India, Email: jbhelonde60@gmail.com
[3]Associate Dean, Department of Electrical and Electronic Engineering, Sandip University, Mahiravani, Nashik, 422213, India, Email: associate.deanengg@sandipuniversity.edu.in
*Corresponding Author: Priyanka Mishra, Research scholar, Department of Electrical and Electronic Engineering, Sandip University, Mahiravani, Nashik, 422213, India, Email: poojamishra1112@gmail.com

Abstract
Optimizing power exchange costs between AC and DC microgrid generators is the primary goal of the study being presented. The recommended concept includes the solar power generating unit, EV charging station, MG controller, and hybrid AC/DC MG system. The AC bus is connected to the electrical load, and the DC bus is attached to WTs, SPV panels, and a charging station. One of the MG controller's other goals is to ensure a steady power flow amongst the system's many components. A momentary graph controller is connected to the charging station and helps regulate the direction of the power flow. A dual converter can be used to convert AC to DC or vice versa. A hybrid AC/DC system needs more care to manage power than either a single AC or DC system, based on cost. The AqMar Algorithm is recommended in order to minimize LPSP and obtain the lowest LCOE. AOA and MPA combined features are used to generate the proposed AqMar technique.

Keywords: Renewable Energy Resources, optimization, Power management

1. Introduction

Micro Grid (MG) is an intriguing option to boost power supply utilization, since it promotes the standard of the electrical energy consumed by various clients and also increases power supply effectiveness [1][2]. Cogeneration systems, also known as Combined Heat and Power (CHP), serve as the best way of achieving Sub Grids (SG) goals amongst various MG configurations. Cogeneration is the concurrent production of both heat and electrical energy from one identical fuel source [3]. The utilization of distributed Renewable Energy Sources (RES) has expanded to mitigate pollution, enhance network dependability, and also to make it easier to electrify remote places [4]. Lately, HRERs, such as Photovoltaic (PV)arrays and Wind Turbine Generators (WTGs), have received a lot of interest [5] because of their potential to decrease carbon emissions, broaden energy sources, and revitalize the local economy, especially in nations that are developing [6] [7][8].

Hybrid MGs provide an effective solution for electrifying impoverished or isolated areas [9] [10]. The growing population and increasing load demand have further promoted the development of sustainable hybrid AC/DC autonomous MGs, especially where grid extension is inadequate or uneconomical [11] [12]. Although long-term ESSs help mitigate HRER fluctuations and support stable MG operation [13] [14], voltage and frequency variations caused by changing environmental conditions still remain a challenge [15]. HESSs, with high power and energy density, effectively manage rapid power fluctuations while maintaining MG reliability and independence [16] [17].

Hybrid AC DC microgrids integrate renewable sources such as PV, wind, biomass, and hydro to enhance system efficiency and reliability [30–38]. EV charging coordination using renewable-powered microgrids improves charging efficiency while stabilizing the DC bus [31, 35, 37]. Advanced control strategies, including adaptive synergy control, address grid impedance variability and maintain system stability [32], while converter-based voltage regulation ensures voltage stability under varying load conditions [33]. Intelligent controllers such as fuzzy logic and ANFIS improve voltage and frequency stability, optimize power sharing, and enhance dynamic response [34,38]. FOPID BFO-based coordinated control further enhances performance under fluctuating renewable generation and load variations [36]. Multi-agent and intelligent voltage control techniques provide efficient reactive power management and power balancing [35].

In recent years, the penetration of EVs and plug-in hybrid EVs in modern power systems has increased significantly [18]. Integrating EVs into renewable energy systems has emerged as an important research area due to challenges related to power management and economic operation [19][20]. Economic assessment considering grid power exchange is also a crucial factor in such systems [21-25]. Moreover, the nonlinear PV characteristics of solar systems necessitate efficient MPPT techniques to enhance power conversion efficiency. With the growing adoption of RES-based DGs such as solar, wind, tidal, biomass, and small hydro systems, reliable MPPT methods are essential for accurately tracking the GMPP within a short time [26] [27] [28]. The growing use of EVs offers possibilities as well as challenges for the current power infrastructure. A smooth power flow among the components, dependability, as well as Automatic Control Systems (ACS) of the system, is the three main design considerations for a renewable energy-based system [29].

The most important objectives of the research are,

- This work presents the design and implementation an AI-based energy management system to monitor and manage the bidirectional power flow between various components in a hybrid renewable energy-based AC/DC microgrid (MG).
- A key objective of the proposed EMS is to minimize the Levelized Cost of Energy (LCOE) during the power exchange between AC and DC microgrids.
- The paper introduces a novel hybrid optimization algorithm named AqMar, which combines the characteristics of two nature-inspired metaheuristic techniques: the Aquila Optimizer (AO) and Marine Predators Algorithm (MPA). This hybrid algorithm is specifically designed to achieve optimal control of power flow within the hybrid AC/DC microgrid.

The remainder of this paper is organized as follows. Section 2 explains the proposed power management strategy, while Section 3 details the AqMar algorithm. Section 4 presents the simulation results and compares the proposed approach with conventional methods. Finally, Section 5 summarizes the conclusions of the work.

2. Proposed Methodology of Power Management

Optimizing power exchange costs among AC as well as DC microgrid generators is the primary goal of the study being presented.

Firstly, unlike conventional microgrid optimization approaches that mainly focus on standalone AC or DC microgrids, the proposed work develops an integrated renewable energy-based hybrid AC/DC microgrid framework consisting of PV systems, wind turbines, EV charging stations, bidirectional converters and coordinated power exchange mechanisms. The proposed method simultaneously addresses power balancing, EV charging coordination and economic energy management within a unified architecture. Secondly, the major contribution of this work lies in the development of the proposed AqMar optimization algorithm, which is a hybrid metaheuristic strategy integrating the exploration capability of the Aquila Optimizer (AO) and the exploitation/search refinement characteristics of the Marine Predators Algorithm (MPA). Existing optimization methods such as PSO, ABC, GWO and standalone AO or MPA often suffer from premature convergence, local optima trapping and inadequate exploration–exploitation balance when solving highly nonlinear microgrid energy management problems. The proposed AqMar algorithm is specifically designed to improve convergence stability, reduce computational time and achieve better optimization accuracy for minimizing LCOE and LPSP simultaneously. Thirdly, unlike many existing studies that mainly optimize either economic cost or reliability independently, the proposed work formulates a coordinated multi-objective energy management strategy considering, LCOE, power exchange cost, Loss of Power Supply Probability (LPSP), EV charging coordination, renewable energy utilization, and bidirectional power flow regulation.

Furthermore, the proposed method demonstrates superior performance in terms of reduced annual system cost, lower LCOE, reduced computational time and improved convergence characteristics compared with several state-of-the-art optimization algorithms. Therefore, the contribution of this work is not merely the application of an existing optimization algorithm, but the development of a hybrid optimization-driven coordinated energy management framework for hybrid AC/DC renewable microgrids with EV integration.

The proposed method includes the solar power generating unit, EV charging station, MG controller, and hybrid AC/DC MG system. The AC bus is connected to the electrical load, and the DC bus is attached to WTs, Solar Photovoltaic (SPV) panels, and a charging station. One of the MG controller's goals is to ensure a steady power flow amongst the system's many components. The MG controller is connected to the charging station, which helps to regulate the direction of the power flow at a specific time. With a dual converter, one can convert AC to DC or vice versa. A hybrid AC/DC system needs more care to manage power than either a single AC or DC system, based on cost. Therefore, the proposed approach integrates smooth power flow among system components with the objective of minimizing overall cost. The AqMar Algorithm is recommended in order to minimize LPSP and obtain the lowest LCOE. AOA [31] and MPA [32] combined features are used to generate the proposed AqMar. The proposed hybrid renewable energy system combines multiple energy sources, leading to a complex optimization problem with several decision-making parameters. The main aim of the proposed approach is to determine the optimal sizing of the converter, wind, and SPV units while minimizing the LCOE and LPSP objectives. To provide a continuous power supply for AC loads and EV charging stations, proper coordination among the available energy sources is essential. Hence, the optimization process considers both economic factors and long-term system performance to achieve an effective balance between LCOE and LPSP. The proposed AqMar algorithm identifies the optimal system configuration by minimizing LCOE while maintaining LPSP within permissible limits, thereby enabling efficient power exchange between the utility grid and other system components. The schematic structure of the proposed system is presented in Figure 1.

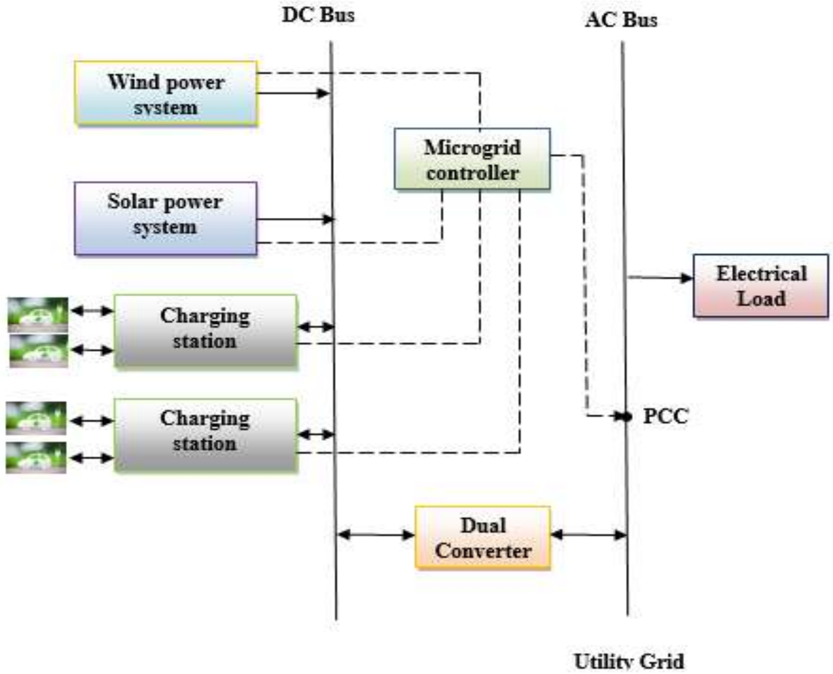

Figure 1. Schematic diagram of the proposed system [39]

2.1 Modelling of wind turbine

The aerodynamic performance of the Inflatable Savonius Wind Turbine (ISWT) is evaluated using numerical simulation because its inflated thick blades differ significantly from the thin rigid blades of conventional Savonius turbines. The ISWT is assumed to be a rigid structure with smooth curved surfaces, and a 2D model is developed in SOLIDWORKS for efficient computation.

The turbine has a central column diameter of 25 cm and an overall diameter of 150 cm. Different models are created by varying the blade thickness (l) and blade arc angle (φ) to study their effects on performance.

The key performance parameters are the tip-speed ratio (λ), static torque coefficient (C_{ts}), dynamic torque coefficient (C_t), and power coefficient (C_p).

The tip-speed ratio is defined s:

$$\lambda = \frac{\omega R}{V} = \frac{n\pi R}{30V} \tag{1}$$

where, ω is the angular velocity, n is the rotational speed, R is the turbine radius, and V is the wind speed.

The static torque coefficient is:

$$C_{ts} = \frac{T_s}{\frac{1}{2}\rho ARV^2} \tag{2}$$

where, T_s is the static torque, ρ is air density, and A is the swept area.

The dynamic torque coefficient is:

$$C_t = \frac{T}{\frac{1}{2}\rho ARV^2} \tag{3}$$

where, T is the dynamic torque generated by the turbine.

The power coefficient, which represents the efficiency of converting wind energy into mechanical power, is expressed as:

$$C_p = \frac{P}{E} = \frac{T.\omega}{\frac{1}{2}\rho ARV^3} = C_t.\lambda \tag{4}$$

where, P is the mechanical power output and E is the kinetic energy of the incoming wind [38].

2.2 SPV Panel

An SPV panel is used to generate electrical power from solar energy. The output power of the SPV panel depends on solar irradiance and cell temperature. The output power of a single SPV panel is given by

$$p_{out}(t) = \frac{P_r G}{1000}\left[1 - \lambda\left(T_c - 25^0 C\right)\right] \quad (5)$$

where, $p_{out}(t)$ is the output power of single SPV panel at time t (W), P_r is the rated power of the SPV panel under standard test condition (W), G is the solar irradiance (W/m^2). The T_c is the cell temperature ^0C, λ temperature coefficient of power ($^0C^{-1}$) and fluctuation in power relation to variations in temperature are provided as,

$$T_c = T_a + \frac{T_n - 20^0 C}{0.8} G \quad (6)$$

where, T_c, T_a, and T_n denote the PV cell temperature, ambient temperature, and nominal operating cell temperature (NOCT), respectively. The nominal operating cell temperature is defined under standard operating conditions corresponding to an ambient temperature of $20^0 C$ and a solar irradiance of 0.8kW/m^2. The average maximum output power of the SPV panel is calculated as follows:

$$P_r = V_r I_r \quad (7)$$

where, V_r and I_r are the maximal voltage (V) and current (A), respectively. Additionally, the total output power generated by the SPV array is computed as overall electricity produced by SPV panels $P_{spvp}(t)$ is computed as follows:

$$P_{spvp}(t) = N_{spvp} P_{out}(t) \quad (8)$$

where, N_{spvp} denotes the number of SPV array in the array t (W), $P_{out}(t)$ represents the output power of single SPV panel (W).

2.3 EV charging station

The two-way converter, recharging ports, and EVs make up the charging station. This station is linked to an MG controller, which helps regulate the path of the power flow at a specific moment. Electric vehicles (EVs) can be charged by their SOC, which is the proportion of a battery's usable capacity to its maximal capacity after being fully charged. It displays the battery's remaining charging efficiency in this manner. The actual restrictions placed on EV charging are expressed numerically as:

$$SOC_{ev}{}^{Min} \le SOC_{ev}(t) \le SOC_{ev}{}^{Max} \quad (9)$$

$$C^{Rate}(t) \le C^{Rate}_{Max} \quad (10)$$

where, $SOC_{ev}{}^{Min}$, $SOC_{ev}{}^{Max}$, and SOC_{ev} t are the minimal, maximal, and existing SOC values for a specific EV at a specific time t, correspondingly; $C^{Rate}(t)$ and C^{Rate}_{Max} are the current charging rate and maximal permitted charging rate of EVs, correspondingly. The power of the EVs at the charging station at any given time is computed as,

$$P_{cs}{}^{ev}(t) = \frac{E_{ev}{}^{CMax} \cdot SOC_{ev}(t)}{100\Delta t} \quad (11)$$

where, $E_{ev}{}^{CMax}$ is the maximal energy capacity of EV(kWh), and Δt is the duration that is represented in hours (h). Evaluating EVs SOC with SOC_{critic} that is the fundamental SOC, which reveals a variance in their recharging needs. In this work, 20 EVs are charged at a charging station using a level 2 charger, which has the merits of being simple and easy to use.

2.4 Power Converter

DC electricity is provided to EVs at the charging station by PV panels and WTs. Conversely, however, converters are necessary to supply power to the grid or to meet load demand. The converter's size is determined by the maximum grid purchase P^{Grid}_{Max} and sales capability P^{pc}_{Max}. The inverter's $P^{in}(t)$ and the rectifier's $P^{re}(t)$ rated powers are calculated as follows:

$$P^{in}(t) = \frac{P_{Max}^{Grid}}{\eta^{in}} \tag{12}$$

$$P^{re}(t) = P_{Max}^{pc} \cdot \eta^{re} \tag{13}$$

where, η^{in} and η^{re} are the effectiveness estimates of the inverter and rectifier, respectively. Figure 2 shows the flowchart of the power management.

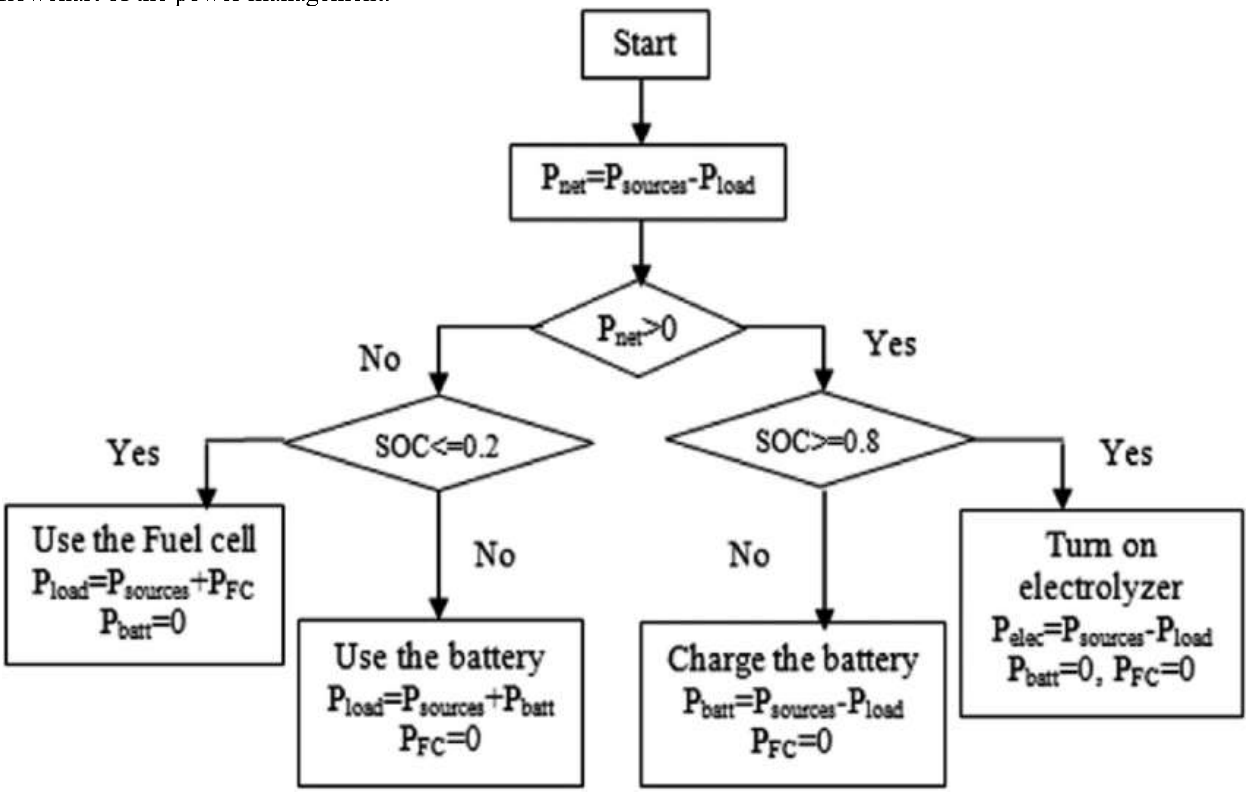

Figure 2. Flowchart of the Power Management

2.5 Operational strategy and objective function

To confirm that the solar-wind hybrid system meets the load power demand N_{spvp} and N_{wind} must be established. Reliability and LCOE are taken into account when formulating the objective function.

A. Reliability

When a network has enough power to meet the load demand, which is dependent on LPSP, it is said to be reliable. Two different load needs must be met: the first is the load demand of Evs $P_{ld}^{ev}(t)$ as well as the second $P_{ld}^{ac}(t)$ is the demand for AC load. Calculating $P_{ld}^{ev}(t)$ at a particular period t is as follows:

$$P_{ld}^{ev}(t) = \frac{E_{ev}^{CMax}.SOC_{critic}}{\Delta t} - P_{cs}^{ev}(t) \tag{14}$$

Two resources, namely SPV panels and the WT, meet these requirements. The formula used to compute the variation between power produced and power demand is:

$$\Delta P(t) = P_{spvp}(t) + P_{wind}(t) - P_{ld}^{ev}(t) - P_{ld}^{ac}(t) / \eta^{re} \tag{15}$$

The cases are organized as follows based on $\Delta P(t)$.

i) If $\Delta P(t) > 0$, the combined output power from the WTs and SPV modules is enough to provide the electric load and charge the EVs. Additionally, the surplus available power $P_{Grid}(t)$ is sold to the grid, which is computed as:

$$P_{Grid}(t) = \left(P_{spvp}(t) + P_{wind}(t) - P_{ld}^{ev}(t)\right)\eta^{in} - P_{ld}^{ac}(t) \tag{16}$$

ii) If $\Delta P(t) > 0$ and $\Delta P(t) > P_{Max}^{Grid}(t)$, the supplementary power is delivered to the dump load, dump power load $P_{ld}^{dump}(t_1)$ is computed as:

$$P_{ld}^{dump}(t) = P_{spvp}(t) + P_{wind}(t) - P_{ld}^{ev}(t) - \left(P_{ld}^{ac}(t) + P_{Max}^{Grid}(t)\right) / \eta^{re} \quad (17)$$

iii) If $\Delta P(t) < 0$, When the power generated by the SPV modules and WTs is insufficient to satisfy the EV and load demand, the required power is supplied by the grid as follows:

$$P^{pc}(t) = \left(P_{ld}^{ev}(t)\right) - P^{wind}(t) - P_{spvp}(t) / \eta^{re} + P_{ld}^{ac}(t) \quad (18)$$

iv) If $\Delta P(t) = 0$, no energy from the grid is exchanged, and the electricity needed for EVs and other electrical loads is produced by SPV modules and WTs. When $P^{pc}(t) > P_{Max}^{pc}(t)$, neither sources nor grids can meet the demands of the loads. As a result, there is an energy shortage, which is computed as,

$$P^{defici}(t) = P^{pc}(t) - P_{Max}^{pc}(t) \quad (19)$$

When lowering the LPSP, $P^{defici}(t)$ it should remain zero to ensure that the entire load demand is continuously met. Mathematically, LPSP can be determined as:

$$LPSP = \frac{\sum_{t=1}^{8760} P^{defici}(t)}{\sum_{t=1}^{8760} \left(P_{ld}^{ac}(t) + P_{ld}^{ev}(t)\right)} \quad (20)$$

To address the optimal sizing problem, the LPSP is maintained within a specified tolerance limit. In this work, the upper limit of LPSP is set to 1%.

2.6 LCOE

The key goals of this article are to establish the transfer of power across multiple system parts and reduce the LCOE of the suggested structure. To keep LPSP and ACS at the bare minimum, the decision variables, such as N_{spvp} and N_{wind} are necessary. The ACS includes the costs associated with SPV module and WT installation, purchasing and selling power to the grid, as well as converter-related expenses.

$$ACS = F\left(N_{spvp}C_{spvp} + N_{wind}C_{wind} + C^{pc}E^{pc} - C^{grid}E^{grid} + C^{co}\right) \quad (21)$$

whereas, C_{spvp} and C_{wind} are the rates of SPV modules and WTs, respectively. Both C^{pc}, C^{grid} define the expense as well as both E^{pc}, E^{grid} defines the quantity, here the superscript *pc* and *grid* indicates gained and delivered energy to the grid, correspondingly, and C^{co} is the rate of the converters. In addition, C_{spvp} and C_{wind} are calculated as:

$$C_{spvp} = C_{can}^{spvp} + C_{rcoa}^{spvp} + C_{opm}^{spvp} + C_{salv}^{spvp} \quad (22)$$

$$C_{wind} = C_{can}^{wind} + C_{rcoa}^{wind} + C_{opm}^{wind} + C_{salv}^{wind} \quad (23)$$

Where, C_{rcoa} is the annual replacement cost, , C_{can} is the annual capital cost, C_{opm} is the maintenance cost and C_{salv} is the salvage value, and the subscripts $wind$ and $spvp$ indicates the WT and SPV, respectively.

i) Annual Capital Cost C_{can} :

Here, the installment and acquisition rates of the essentials are also incorporated. C_{can} of SPV module and WTs, denoted as C_{cai}^{spvp} and C_{cai}^{wind}, correspondingly are computed by introducing the capital recovery factor $f_{A/P}$ and are as follows:

$$C_{can}^{spvp} = C_{cai}^{spvp} \cdot f_{A/P}\left(t_p, r_{an}\right) \quad (24)$$

$$C_{can}^{wind} = C_{cai}^{wind} \cdot f_{A/P}\left(t_p, r_{an}\right) \quad (25)$$

$$f_{A/P}\left(t_p, r_{an}\right) = \frac{t_p\left(1 + t_p\right)^{r_{an}}}{\left(1 + t_p\right)^{r_{an}} - 1} \quad (26)$$

ii) Annual replacement Cost C_{rcoa}

This cost further considers the replacement of SPV modules and WTs if their service life is shorter than the project period. The annual replacement cost of the SPV panels and wind turbine is calculated as follows:

$$C_{rcoa}^{spvp} = C_{rco}^{spvp} \cdot f_{A/P}\left(t_p, r_{an}\right) \cdot \frac{1}{\left(1+t_p\right)^{\tau}} \tag{27}$$

$$C_{rcoa}^{wind} = C_{rco}^{wind} \cdot f_{A/P}\left(t_p, r_{an}\right) \cdot \frac{1}{\left(1+t_p\right)^{\tau}} \tag{28}$$

where, C_{rco}^{wind} as well as C_{rco}^{spvp} are the costs of replacing the wind turbine and the SPV panel and τ is the lifetime of the panel and WT in years.

iii) Maintenance Cost C_{opm}

This includes the cost of labor, and renovation in case of any temporary damage. C_{opm1}^{wind} and C_{opm1}^{spvp} are the maintenance costs of wind turbine and SPV panel, correspondingly and are found as:

$$C_{opm}^{spvp} = N_{spvp} \cdot C_{opm1}^{spvp} \tag{29}$$

$$C_{opm}^{wind} = N_{spvp} \cdot C_{opm1}^{wind} \tag{30}$$

iv) Salvage Value

The residual value of the module at the end of the project lifetime is referred to as the salvage value. The salvage values of a WT and SPV panel, where C_{rco}^{spvp} and C_{rco}^{wind} are the replacement costs of a single SPV panel as well as wind turbine respectively.

$$C_{salv}^{wind} = C_{rco}^{wind} \cdot \frac{\Gamma_{remain}}{\tau} \tag{31}$$

$$C_{salv}^{spvp} = C_{rco}^{spvp} \cdot \frac{\Gamma_{remain}}{\tau} \tag{32}$$

where, Γ_{remain} is the residual time.

v) Cost of Exchanging Power

The quantity of energy gained E^{pc} and delivered to the grid E^{grid} can be computed as:

$$E^{pc} = \sum_{t_1=1}^{86400} P^{pc}(t) \tag{33}$$

$$E^{grid} = \sum_{t_1=1}^{86400} P^{grid}(t) \tag{34}$$

The expense of energy gained E^{pc} and delivered to the grid E^{grid} can be found as:

$$C^{pc} = E^{pc} \cdot C_{unit}^{epu} \tag{35}$$

$$C^{grid} = E^{grid} \cdot C_{unit}^{esb} \tag{36}$$

where, C_{unit}^{esb} and C_{unit}^{epu} are the unit costs of energy delivered as well as gained to the grid, respectively. The objective function, LCOE, represents the average cost of energy produced by the system and is used to evaluate its economic performance. It is formulated as follows: $LCOE = \dfrac{ACS}{\rho_{tot}}$ (37)

where, ρ_{tot} is the overall energy conserved. The constraints are given as:

$$1 \le N_{spvvp} \le N_{Max}^{spvp} \tag{38}$$

$$1 \le N_{wind} \le N_{Max}^{wind} \tag{39}$$

$$\begin{cases} P_{pc} \le P_{Max}^{pc} \\ P^{grid} \le P_{grid}^{Max} \end{cases} \tag{40}$$

$$0 \le LPSP \le 1\% \tag{41}$$

where, $\rho_{tot} = 6.0045e^{6}$, N_{Max}^{spvp} and N_{Max}^{wind} are the maximum numbers of SPV modules and WTs, correspondingly [30].

3. Proposed AqMar Optimizer

The proposed AqMar optimizer is not a direct application or sequential combination of Aquila Optimizer (AO) and MPA. Instead, the proposed method introduces a coordinated hybrid search method specifically designed for solving the nonlinear and highly constrained hybrid AC/DC microgrid energy management problem. The novelty of AqMar lies in the adaptive integration of the exploration and exploitation mechanisms inherited from AOA and MPA to improve convergence stability and global search capability.

In conventional AOA, strong exploration capability exists during the initial search stages; however, the algorithm may experience unstable exploitation behavior and slower convergence near the global optimum. Similarly, MPA demonstrates effective local exploitation capability but may suffer from reduced population diversity and local optimum trapping under high-dimensional optimization problems. To overcome these limitations, the proposed AqMar method introduces, adaptive switching between Aquila exploration and Marine Predator exploitation phases, improved population update strategy, enhanced exploration–exploitation balance, and dynamic convergence refinement for renewable energy optimization problems.

Unlike standalone AOA or MPA, the proposed AqMar optimizer modifies the search transition mechanism such that the global exploration behavior of Aquila hunting is adaptively coordinated with the localized predatory movement characteristics of MPA. This adaptive coordination improves population diversity during early iterations while simultaneously enhancing convergence precision during later iterations. Consequently, the proposed approach reduces premature convergence and improves solution stability for minimizing LCOE and LPSP simultaneously [40]. The subsequent actions represent the AO method's framework for hunting procedures:

Solution Initialization:

Every optimization technique' solution begins with arbitrary solutions of candidate solutions $\left(\Pi_{mn}\right)$ in the range between upper $\left(ul_n\right)$ and lower limits $\left(ll_n\right)$, as seen in the following expression:

$$\Pi_{mn} = arb \times \left(ul_n - ll_n\right) + ll_n \tag{42}$$

Whereas, arb is an arbitrary number, ll_n indicates the n^{th} lower limit, and ul_n indicates the n^{th} upper limit of the given problem.

Step 1: Expanded Exploration (Π_1)

To begin with, Aquila investigates any possible prey in the search area. Expanded exploration is the term used in the search space for this exploration activity, which is carried out at high altitudes. The Aquila stoops vertically to drop and catch its prey after it has explored it. In mathematical terms, this pattern of action is replaced with the MPA [41] as follows:

$$\Pi_1 = \Pi_{Best_m} + Q \cdot A \otimes stepsize \tag{43}$$

Whereas, $stepsize = A_{brow} \otimes \left(elit_m - A_{brow} \otimes \Pi_{Best_m}\right)$, $A_{brow} = arbn(\mathrm{M}, di)$ and Brownian motion is represented by the vector A_{brow}, which contains arbitrary numerals with normal distribution. The notation $\otimes$ denotes entry-wound multiplications. The product of A_{brow} and Π_{Best_m} simulates the progress. $Q = 0.5$ and A denotes a vector of constant arbitrary numerals in [0, 1].

Step:2 Narrowed Exploration $\left(\Pi_2\right)$

The second method, hunting at contour flight with a brief glide attack, is the one that Aquila employs the most. As a result, the Aquila is near the pursued prey, which causes a limited search area to be explored. This procedure is envisioned as:

$$\Pi_2(g+1) = \Pi_{Best}(g) \times L(di) + \Pi_a(g) + (p-q) \times arb \tag{44}$$

where, $\Pi_a(g)$ is an arbitrary solution interpreted at the m^{th} iteration. Utilizing the subsequent formula, the Levy flight function $L(di)$ of distribution for the dimensional space (di) is found as:

$$L(di) = x \times \frac{j \times \gamma}{|k|^{1/\alpha}} \tag{45}$$

where, $x = 0.01$ (constant value), j and k are arbitrary values between 0 and 1. γ is a dynamic, adaptable coefficient which is found as follows:

$$\gamma = \left(\frac{\delta(1+\alpha)\times sin\left(\frac{\pi\alpha}{2}\right)}{\delta\left(\frac{1+\alpha}{2}\right)\times\alpha\times 2^{\left(\alpha-\frac{1}{2}\right)}} \right) \tag{46}$$

Where $\alpha = 1.5$. The coiled shape of the procedure for exploration is determined by the values of p and q , which can be calculated as shown below:

$$p = s\times cos(\theta) \tag{47}$$

$$q = s\times sin(\theta) \tag{48}$$

$$s = s_1 + \mathrm{O}\times di_1 \tag{49}$$

$$\theta = -\mathrm{M}\times di_1 + \theta_1 \tag{50}$$

$$\theta_1 = 3\times\frac{\pi}{2} \tag{51}$$

In which s_1 ranges between 1 and 20, O = 0.00565, The search space's dimensionality is represented by the integers di_1, starting at 1 and M =0.005.

Step 3: Expanded Exploitation (Π_3)

The third method is the expanded exploitation of any grounding prey with a lethargic escaping reflex. Aquila hovers at a low altitude, and once it has chosen its target, it slowly descends to attack it. This phase is described numerically under the following circumstances through the MPA model [41]:

$$\Pi_3 = \mathrm{elit}_m + \mathrm{Q.cf}\otimes \mathrm{stepsize}_m \tag{52}$$

$$\mathrm{cf} = \left(1-\frac{\mathrm{itn}}{\mathrm{MAX}_{\mathrm{itn}}}\right)^{\left(2\frac{\mathrm{itn}}{\mathrm{MAX}_{\mathrm{itn}}}\right)} \tag{53}$$

where,

$$\mathrm{stepsize}_m = \mathrm{A}_{\mathrm{brow}} \otimes \left(\mathrm{A}_{\mathrm{brow}}\otimes \mathrm{elit}_m - \mathrm{prey}_m\right) \tag{54}$$

else

$$\Pi_3 = \mathrm{elit}_m + \mathrm{Q.cf}\otimes \mathrm{stepsize}_m \tag{55}$$

where, $\mathrm{stepsize}_m = \mathrm{A}_L \otimes \left(\mathrm{A}_L \otimes \mathrm{elit}_m - \mathrm{prey}_m\right)$ (56)

Here, cf is being regarded as an adaptable variable to regulate the predator's motion step size. Prey changes its position based on a predatory move in Brownian motion, whilst the product of $\mathrm{A}_{\mathrm{brow}}$ and elit_m replicates this instance. A_L is a vector of arbitrary values. Adding the step size to the prey location represents the motion of the prey, multiplying A_L and elit_m replicating the motion of the prey in a Levy fashion.

Step 4: Narrowed Exploitation (Π_4)

The fourth procedure involves the movement of Aquila across the ground and dragging its prey into its mouth. It is referred to as a narrowed exploitation stage and is employed for dealing with huge prey. The mathematical model for this step is:

$$\Pi_4(g+1) = \mathrm{qf}\times\Pi_{\mathrm{Best}}(g) - (\mathrm{H}_1\times\Pi(g)\times\mathrm{arb}) - \mathrm{H}_2\times\mathrm{L}(\mathrm{di}) + \mathrm{arb}\times\mathrm{H}_1 \tag{57}$$

Here qf is a qualitative function that is determined as in Eqn. (58) and is used to equilibrate searching tactics. H_1 represents multiple AO movements, which are produced by Eqn. (59). H_2 is the aerial gradient of AO, which is represented by Eqn. (60) and has a value lowering from 2 to 0 throughout the prey's lope from its initial to the final location.

$$\mathrm{qf}(g) = g^{\frac{2\times\mathrm{arb}(\ )-1}{(1-G)^2}} \tag{58}$$

$$H_1 = 2\times arb(\ )-1 \tag{59}$$

$$H_2 = 2\times\left(1-\frac{g}{G}\right) \tag{60}$$

where, $\mathrm{qf}(g)$ is the qualitative function at the g^{th} iteration, and arb is an arbitrary numeral ranging amid 0 and 1. g and G are the present and maximal number of iterations, correspondingly.

Pseudo-code of AqMar Optimizer

To summarize, in AO, the method of optimization begins the enhancement process by creating a randomly established population of potential solutions. The searching tactics of the AO examine the feasible places of the best-obtained solution or the close-to-optimal solution along the trajectory of repetition. Each solution modifies its placements following the optimal result produced by the AO's methods of optimization. Four alternate search techniques for exploration and exploitation, namely, expanded and narrowed exploration, expanded and narrowed exploitation are offered to highlight the equilibrium that exists among AO's methods of searching (i.e., exploration and exploitation). When the end criterion is satisfied, the search procedure of the AO is finally accomplished.

4. Results and Discussion

4.1 Simulation Setup

The suggested AI-based energy management system with the Novel Hybrid Optimization Technique in EVs was implemented using MATLAB 2021b. The simulation graphs are acquired for ACS, Convergence, Cost of SPV and WT, power of EV, PV and WT, LCOE, Solar radiation, wind speed, and Exchange of SPV and WT respectively. In this instance, the efficacy of existing methodologies, such as PSO [33], ABC [34], GWO [35], AQO [22], Kookaburra Optimization Algorithm (KOA) [36], Gazelle Optimization Algorithm (GOA) [37] and MA [25] was assessed. The effectiveness of the proposed method in efficient energy management is validated by comparing its performance metrics with those of conventional approaches. The results are analyzed for load demand values of $6 \times 10^6 + 4.4 \times 10^{16}$ and $7\times 10^6+5\times 10^{16}$. Table 1 illustrates the specifications of SPV panel and wind turbine.

Table 1: Specifications of SPV Panel and Wind Turbine

Component	**Rating**
SPV Panel	100 W
Wind Turbine (WT)	1 kW

4.2 Optimal configuration of the power source

Table 2: Optimal configuration of SPVs and WT used in conventional and proposed methodologies

Methods	**No. of SPV**	**No. of WT**
PSO	2	3
ABC	3	3
GWO	6	4
AQO	8	5
MA	9	5
KOA	9	3
GOA	8	1
PROP	1	1

Table 2 portrays the number of SPVs and WTs used in conventional methodologies, such as PSO, ABC, GWO, AQO, MA, KOA, GOA and the suggested AqMar method. In the method of PSO, 2 SPVs and 3WTs are used, in ABC, 3 SPVs and 3WTs are used, in GWO, 6 SPVs and 4WTs are used, in AQO, 8 SPVs and 5 WTs are used, in MA 9 SPVs and 5 WTs, in KOA 9 SPVs and 1 WT are used, in GOA 8 SPVs and 1WTs are used, whereas for AqMAr, only one SPV and only one WT is used.

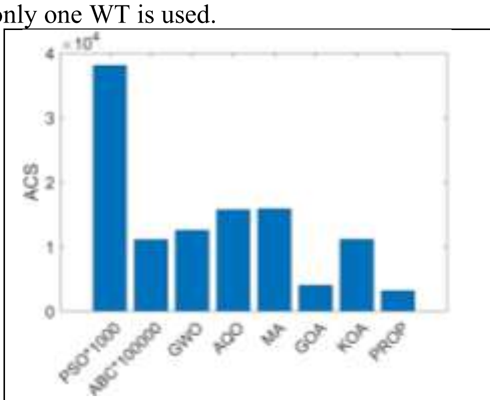	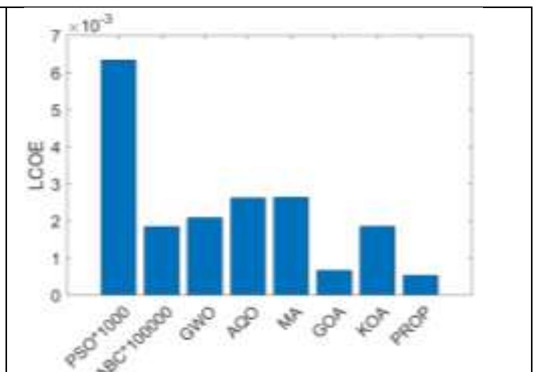
a)ACS	b)LCOE

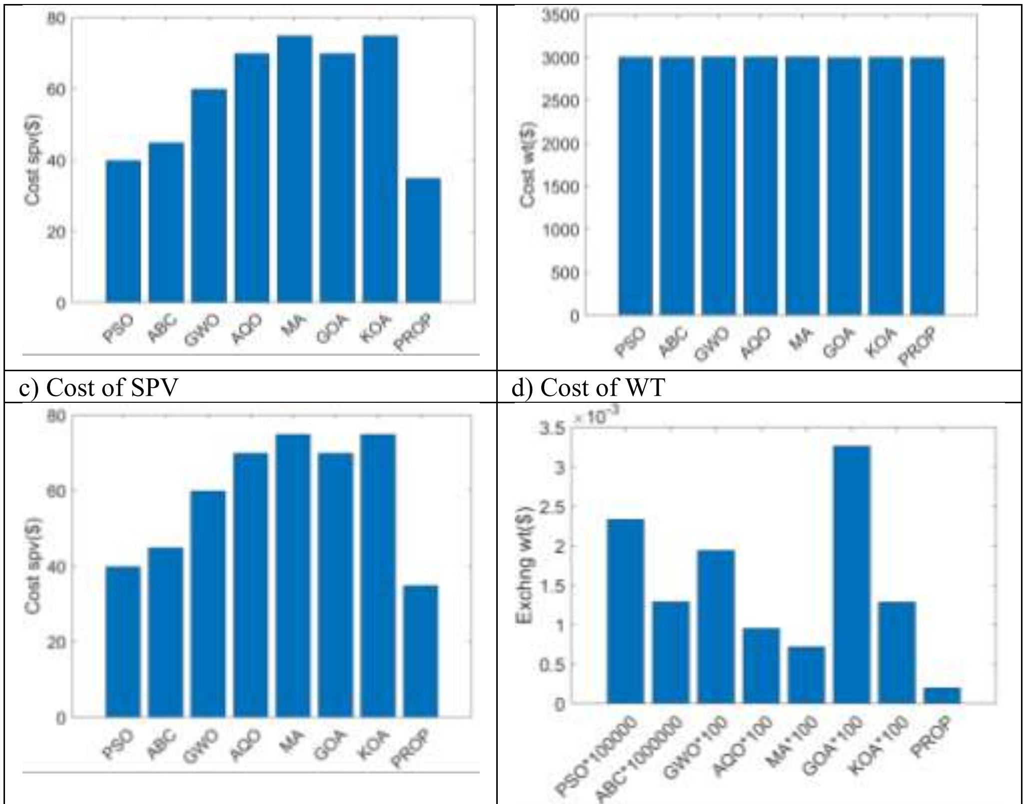

c) Cost of SPV

d) Cost of WT

e)Cost of exchanging power of SPV

f) Cost of exchanging power of WT

Figure 3. Comparison of optimal parameters of various conventional methodologies to that of the suggested technique

Fig. (3) shows the comparison of optimal parameters of various conventional methodologies to that of the suggested technique. The suggested AqMar methodology yields the lowest cost of SPV with 34.82 whereas for PSO it is 39.82, for ABC it is 44.82, for GWO it is 59.82, for AQO it is 69.82, for MA it is 74.82, KOA it is 69.82, and GOA it is 74.82 as shown in Table.3. Additionally while considering the cost of WT for various conventional methodologies and the suggested AqMar approach, PSO yields 3000.5, ABC yields 3000.5, GWO yields 3002.5, AQO yields 3004.5, MA yields 3004.5, KOA yields 2996.5 and GOA yields 3000.5 while for AqMar it is 2996.5.

Table 3: Optimal Parameters when load demand is $6 \times 10\times6 + 4.4 \times 10\times16$

	PSO	**ABC**	**GWO**	**AQO**	**MA**	**KOA**	**GOA**	**PROP**
ACS per year($/year**)**	3.8081×10^{7}	1.1081×10^{9}	12522	15714	15826	3987.8	1.1128×10^{9}	3158.3
LCOE($/kWh**)**	6.342	184.54	0.0020855	0.0026171	0.0026357	0.00066	185.34	0.000526
Cost of SPV($/year**)**	39.82	44.82	59.82	69.82	74.82	69.82	74.82	34.82
Cost of WT($/year**)**	3000.5	3000.5	3002.5	3004.5	3004.5	2996.5	3000.5	2996.5
Cost of exchanging power of SPV($/year**)**	673.92	3663.9	0.56043	0.27466	0.20305	1.640	3667.7	0.000333
Cost of exchanging power of WT($/year**)**	233.28	1286.5	0.1939	0.095157	0.071464	0.3259	1285.2	0.000197

While considering the cost of exchanging power of SPV and WT, the conventional methodologies, namely PSO, acquire 673.92 and 233.28, ABC acquires 3663.9 and 1286.5, GWO acquires 0.56043 and 0.1939, AQO acquires 0.27466 and 0.095157, MA acquires 0.20305 and 0.071464, respectively. However, the suggested method achieved very low values of 0.00033256 and 0.00019677. LPSP can be minimized and the lowest LCOE can be found by utilizing the AqMar Algorithm. The suggested AqMar is generated by combining features from AOA and MPA. Consequently, the low-fitness values required by the simulation study can be met by modifying the suggested AqMar technique, which yields lower fitness values than the traditional procedures. Hence, it is evident that the cost of WT in the proposed approach is much less when compared to other approaches. Table 4 below shows the capacity of production of WT, SPV, EV load of PSO, ABC, GWO, AQO, MA, KOA, GOA and the proposed methodology, whereas Table 5 shows the computational time of conventional and suggested approaches.

Table 4: Production capacity of various conventional methodologies and AqMar when load demand is $6 \times 10^6 + 4.4 \times 10^{16}$

	PSO	**ABC**	**GWO**	**AQO**	**MA**	**KOA**	**GOA**	**PROP**
WT production(kWh)	1.0096×10^9	1.0096×10^9	1.3461×10^9	1.6827×10^9	1.6827×10^9	3.3653e+08	1.0096e+09	3.3653×10^8
SPV production(kWh)	4.0317×10^{10}	6.0476×10^{10}	1.2095×10^{11}	1.6127×10^{11}	1.8143×10^{11}	1.6127e+11	1.6127e+11	2.0159×10^{10}
EV load production(kWh)	60.153	60.203	60.067	60.131	60.125	60.163	59.779	60.22

Table 5: Computational time of conventional vs suggested approaches

Methods	Computational time(sec)
PSO	78.121
ABC	84.21
GWO	86.506
AQO	193.63
MA	176.24
KOA	76.852
GOA	79.516
PROP	64.736

The computational time of PSO is 78.121, for ABC it is 84.21, for GWO it is 193.63, for MA it is 176.24, for KOA it is 76.85, for GOA it is 79.51, and for the recommended AqMar approach it is 64.736. The solar radiance and wind speed of the suggested approach are shown in Figure 4.

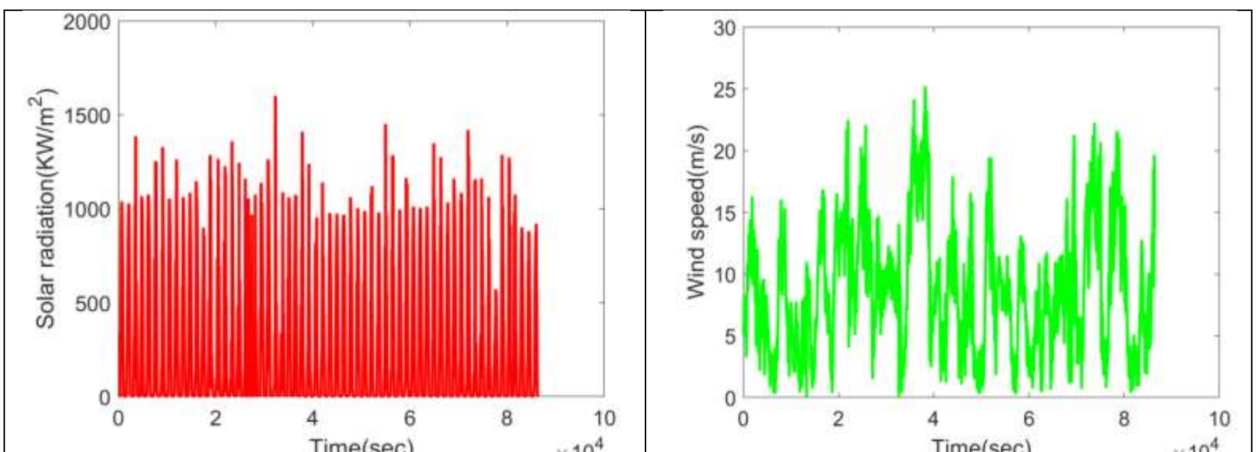

a) b)

Figure 4. Solar radiation and wind speed analysis of the suggested approach

4.3 Convergence Analysis

The convergence analysis helps to determine how fast the proposed algorithm approaches the solution, which is crucial for efficiency. The suggested technique and conventional methodologies in terms of fitness values are contrasted in

Figure 5. Hence, by analyzing the fitness values of various conventional methodologies with those of the suggested technique, it is evident that the suggested AqMar approach constantly delivers the least fitness values. The proposed method attains the fitness values of 3971.5, 3159.3, and 3158.3 in the 10th, 20th and 100th iteration, respectively, that are less than those of the values obtained from various conventional methodologies, such as PSO, ABC, GWO, AQO, KOA, GOA and MA, accordingly. The suggested approach at the 20th iteration is 99.99%, 99.99%, 1.45%, 1.09%, 2.93%, 99.99%, and 40.76% higher than the traditional models like PSO, ABC, GWO, AQO, KOA, GOA and MA, respectively. Similarly, at the 80th iteration, the proposed method is 99.99%, 99.99%, 1.44%, 1.09%, 2.93%, 99.99%, and 40.77% better than the existing models like PSO, ABC, GWO, AQO, KOA, GOA and MA, respectively. These results indicate that the proposed AqMar approach not only converges efficiently but also consistently achieves lower fitness values, demonstrating high convergence accuracy.

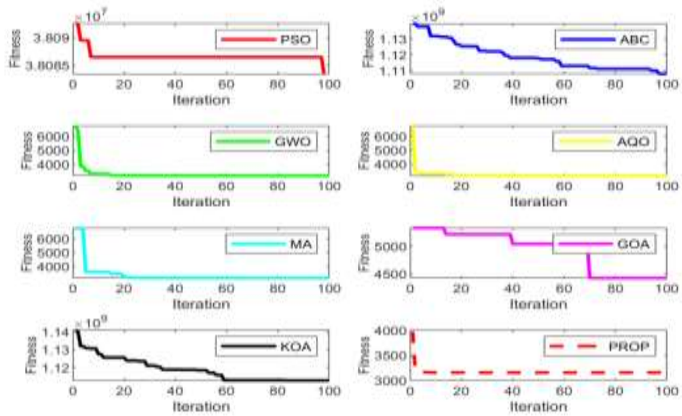

Figure 5. Convergence analysis of AqMar over different traditional approaches

4.4 Exchange power characteristics of the proposed AqMar method

Fig. 6 presents the hourly exchange power characteristics of the SPV and WT units under the proposed AqMar optimization strategy. The results indicate that the exchange power between the renewable sources and the hybrid AC/DC microgrid remains stable throughout the 24-hour operating period. The hourly exchange power profile deviation of SPV is approximately 1.36×10^{-3} to 1.42×10^{-3}, while the WT exchange power ranges between 1.37×10^{-3} and 1.43×10^{-3}. These variations occur due to the intermittent nature of solar irradiance and wind speed.

The obtained exchange power profile confirms that the proposed AqMar technique effectively regulates the bidirectional power flow between the AC and DC buses while satisfying the load demand constraints. The smooth exchange characteristics demonstrate that the MG controller successfully minimizes sudden power fluctuations and maintains continuous energy balance within the microgrid system.

Furthermore, the results validate that the Load Probability Supply Probability (LPSP) constraint is properly enforced in the optimization method. The optimized operation reduces unmet load conditions by maintaining coordinated energy sharing between SPV, WT, EV charging station, and the utility grid. Due to the effective utilization of renewable energy sources and controlled exchange power, the dependency on grid purchase/sale becomes significantly lower in the proposed AqMar approach. Hence, the near-zero grid exchange observed in the results is achieved through optimal renewable resource scheduling rather than constraint violation. Overall, the exchange power analysis confirms that the proposed AqMar methodology ensures reliable power management, reduced power mismatch, minimized unmet load, and improved operational stability of the hybrid AC/DC microgrid system.

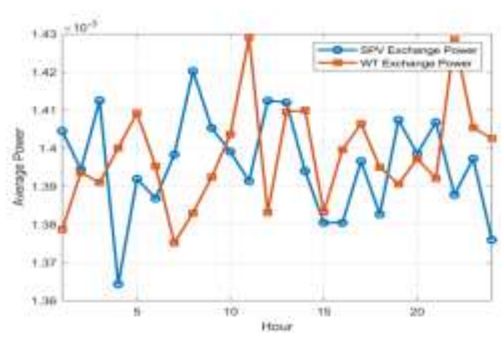

Figure 6. Hourly exchange power profile deviation of SPV and WT units in the proposed AqMar-based hybrid AC/DC microgrid system, when meeting the load demand

4.5 Benchmark Validation of AqMar Using CEC Functions

Figures 7(a)–(h) present the convergence characteristics of the proposed AqMar algorithm compared with PSO, ABC, GWO, AQO, MA, GOA, and KOA using different CEC 2022 benchmark functions [39]. From Figure7 (a), the proposed AqMar algorithm converges to the minimum fitness value within nearly 40–50 iterations, whereas PSO, ABC, GWO, AQO, MA, GOA, and KOA require approximately 120, 95, 80, 70, 65, 60, and 85 iterations, respectively. The faster convergence rate of AqMar indicates its superior global search capability and reduced computational effort. Similarly, in Figure 7(b), AqMar achieves stable convergence within nearly 55 iterations, while PSO requires more than 160 iterations to approach the optimal solution. ABC, GWO, AQO, MA, GOA, and KOA converge within approximately 110, 95, 82, 75, 68, and 90 iterations, respectively. The reduced iteration count demonstrates the enhanced convergence stability and optimization efficiency of the proposed method.

Figures 7(c) and 7(d) further confirm the superiority of AqMar in terms of convergence speed and fitness minimization. In Figure 7 (c), AqMar reaches the optimal fitness value in nearly 35 iterations, whereas the compared algorithms require more than 60–120 iterations. Likewise, in Figure 7 (d), AqMar converges within approximately 45 iterations, while GWO and KOA require nearly 140 and 120 iterations, respectively, to achieve similar fitness levels. For the highly nonlinear benchmark functions shown in Figures 7(e)–(h), the proposed AqMar algorithm exhibits significantly improved optimization performance. In Figure 7(e), AqMar converges within approximately 60 iterations, whereas MA requires nearly 180 iterations due to slower exploitation capability. In Figure 7(f), AqMar attains the minimum fitness value in nearly 50 iterations, while PSO and KOA require more than 110 iterations. Similarly, in Figures 7(g) and 7(h), AqMar consistently achieves rapid convergence within approximately 40–55 iterations, whereas conventional algorithms exhibit delayed convergence and higher fitness fluctuations.

Overall, the numerical convergence analysis clearly demonstrates that the proposed AqMar algorithm provides improved convergence speed, better fitness minimization, and enhanced robustness compared with conventional optimization techniques. The superior performance is mainly attributed to the effective hybridization of Arithmetic Optimization Algorithm (AOA) and Marine Predators Algorithm (MPA), which improves both exploration and exploitation capabilities while preventing premature convergence in complex multimodal optimization problems.

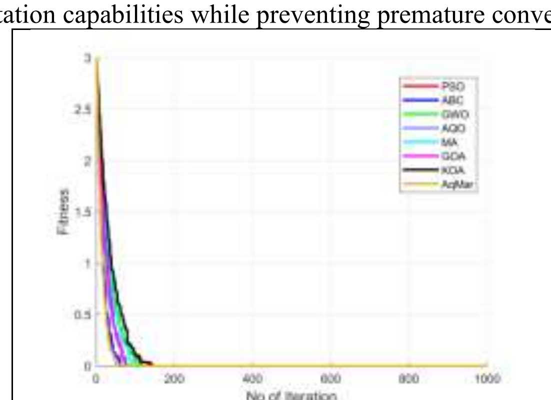

(a)

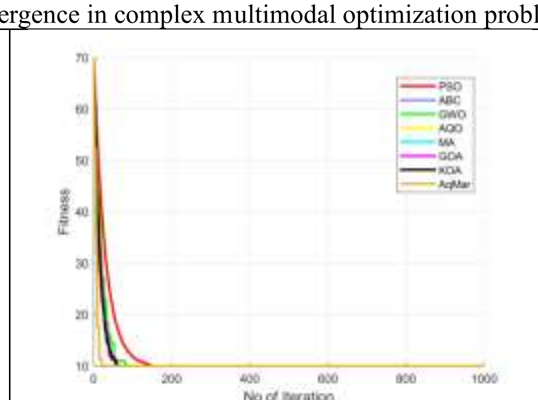

(b)

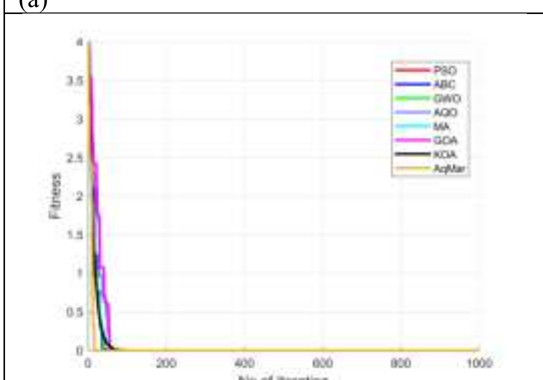

(c)

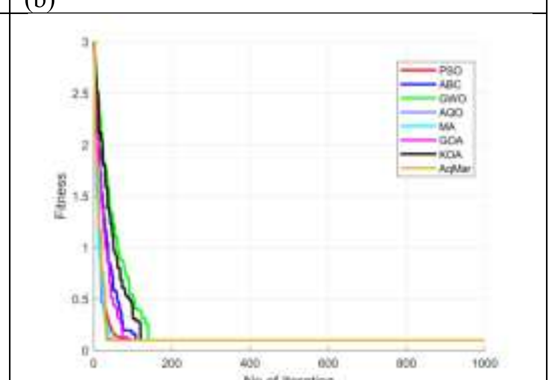

(d)

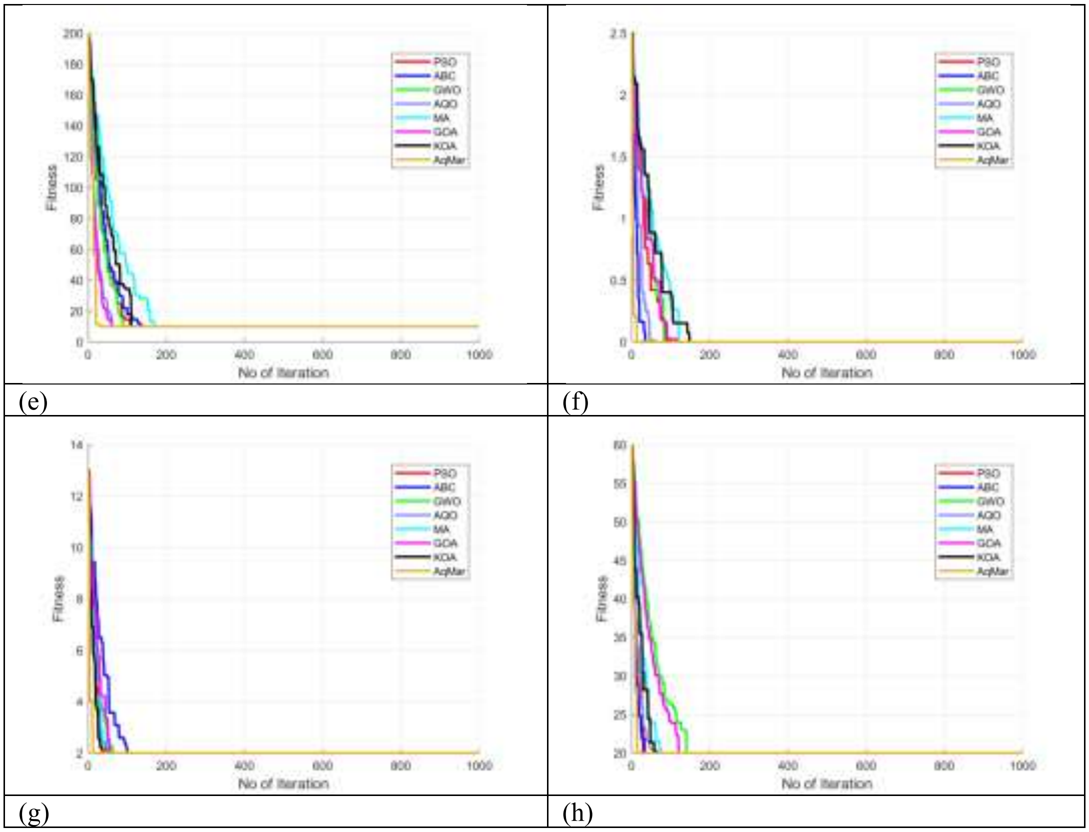

Figure 7. Comparative convergence performance of PSO, ABC, GWO, AQO, MA, GOA, KOA, and the proposed AqMar algorithm using CEC 2022 benchmark suites (a) F_1, (b) F_2, (c) F_3, (d) F_4, (e) F_5, (f) F_6 (g) F_7 and (h) F_8

5. Conclusion

Electricity may be consistently and affordably supplied to grid-connected and off-grid conditions using HRESs. The suggested AI-based energy management system with the Novel Hybrid Optimization Technique in EVs was implemented using MATLAB 2021b. The suggested AqMar methodology yields the lowest cost of SPV with 34.82, whereas for PSO it is 39.82, for ABC it is 44.82, for GWO it is 59.82, for AQO it is 69.82, and for MA it is 74.82. Additionally, while considering the cost of WT for various conventional methodologies and the suggested AqMar approach, PSO yields 3000.5, ABC yields 3000.5, GWO yields 3002.5, AQO yields 3004.5, and MA yields 3004.5, while for AqMar it is 2996.5. Future work will be geared towards extending the fundamental concepts of this study to use with multiple sources and EVs that are intermittent in nature. For use in AC micro-grids and hybrid microgrids, future research should focus on identifying the hybrid algorithm's quick reaction features and investigating the impact of quick battery charging and discharging.

References

1. Ding, Ming, Yingyuan Zhang, and Meiqin Mao. "Key technologies for microgrids-a review." In 2009 International Conference on Sustainable Power Generation and Supply, pp. 1-5. IEEE, 2009.
2. Rathore, Vishal, Krishna Bihari Yadav, and Vikas Kumar. "Modeling and simulation of micro-grid system components." Proceedings of the International Conference on Advances in Electronics, Electrical & Computational Intelligence (ICAEEC). 2019.
3. Kumar, C., and T. Dharma Raj. "A New Nonisolated High-Step-Up DC–DC Converter Topology with High Voltage Gain Using Voltage Multiplier Cell Circuit for Solar Photovoltaic System Applications." Journal of Circuits, Systems and Computers 30, no. 01 (2021): 2150014.
4. Jithendranath, J., Debapriya Das, and Josep M. Guerrero. "Probabilistic optimal power flow in islanded microgrids with load, wind and solar uncertainties including intermittent generation spatial correlation." Energy 222 (2021): 119847.
5. Wang, Richard, Shu-Chien Hsu, Saina Zheng, Jieh-Haur Chen, and Xuran Ivan Li. "Renewable energy microgrids: Economic evaluation and decision making for government policies to contribute to affordable and clean energy." Applied Energy 274 (2020): 115287.
6. Li, Xiangke, Chaoyu Dong, Wentao Jiang, and Xiaohua Wu. "An improved coordination control for a novel hybrid AC/DC microgrid architecture with combined energy storage system." Applied Energy 292 (2021): 116824.
7. Rathore, Vishal, et al. "Load Frequency Control of Multisource Interconnected System Using a Nature-Inspired Optimization Algorithm." TENCON 2025-2025 IEEE Region 10 Conference (TENCON). IEEE, 2025.

8. Bai, J. Johncy, T. S. Sivarani, and M. Dhiviya Nycil. "Optimal Sizing of Grid-Connected HRES with and Without EV using Adaptive-Dwarf Mongoose Optimization Technique." In 2023 5th International Conference on Inventive Research in Computing Applications (ICIRCA), pp. 1765-1772. IEEE, 2023.
9. Xiao, Qian, Yunfei Mu, Hongjie Jia, Yu Jin, Kai Hou, Xiaodan Yu, Remus Teodorescu, and Josep M. Guerrero. "Modular multilevel converter based multi-terminal hybrid AC/DC microgrid with improved energy control method." Applied Energy 282 (2021): 116154.
10. John, Bony, and James Varghese. "Sizing and techno-economic analysis of hydrokinetic turbine based standalone hybrid energy systems." Energy 221 (2021): 119717.
11. Vasudevan, Krishnakumar R., Vigna K. Ramachandaramurthy, Gomathi Venugopal, J. B. Ekanayake, and S. K. Tiong. "Hierarchical frequency control framework for a remote microgrid with pico hydel energy storage and wind turbine." International Journal of Electrical Power & Energy Systems 127 (2021): 106666.
12. Mishra, Sakshi, Kate Anderson, Brian Miller, Kyle Boyer, and Adam Warren. "Microgrid resilience: A holistic approach for assessing threats, identifying vulnerabilities, and designing corresponding mitigation strategies." Applied Energy 264 (2020): 114726.
13. Clarke, Will Challis, Michael John Brear, and Chris Manzie. "Control of an isolated microgrid using hierarchical economic model predictive control." Applied Energy 280 (2020): 115960.
14. Dehghani, Moslem, Abdollah Kavousi-Fard, Taher Niknam, and Omid Avatefipour. "A robust voltage and current controller of parallel inverters in smart island: A novel approach." Energy 214 (2021): 118879.
15. Gargari, Milad Zamani, Mehrdad Tarafdar Hagh, and Saeid Ghassem Zadeh. "Preventive maintenance scheduling of multi energy microgrid to enhance the resiliency of system." Energy 221 (2021): 119782.
16. Mukhopadhyay, Bineeta, and Debapriya Das. "Optimal multi-objective expansion planning of a droop-regulated islanded microgrid." Energy 218 (2021): 119415.
17. Elsisi, Mahmoud, NajmehBazmohammadi, Josep M. Guerrero, and Mohamed A. Ebrahim. "Energy management of controllable loads in multi-area power systems with wind power penetration based on new supervisor fuzzy nonlinear sliding mode control." Energy 221 (2021): 119867.
18. Tamalouzt, S., N. Benyahia, T. Rekioua, D. Rekioua, and R. Abdessemed. "Performances analysis of WT-DFIG with PV and fuel cell hybrid power sources system associated with hydrogen storage hybrid energy system." International journal of hydrogen energy 41, no. 45 (2016): 21006-21021.
19. Faramarzi, Afshin, Mohammad Heidarinejad, SeyedaliMirjalili, and Amir H. Gandomi. "Marine Predators Algorithm: A nature-inspired metaheuristic." Expert systems with applications 152 (2020): 113377.
20. Abualigah, Laith, Dalia Yousri, Mohamed Abd Elaziz, Ahmed A. Ewees, Mohammed AA Al-Qaness, and Amir H. Gandomi. "Aquila optimizer: a novel meta-heuristic optimization algorithm." Computers & Industrial Engineering 157 (2021): 107250.
21. Prasad, T. Narasimha, S. Devakirubakaran, S. Muthubalaji, S. Srinivasan, B. Karthikeyan, R. Palanisamy, Mohit Bajaj, Hossam M. Zawbaa, and Salah Kamel. "Power management in hybrid ANFIS PID based AC–DC microgrids with EHO based cost optimized droop control strategy." *Energy Reports* 8 (2022): 15081-15094.
22. Abou El-Ela, Adel A., Ragab A. El-Sehiemy, Abdullah M. Shaheen, and Ayman S. Shalaby. "Aquila optimization algorithm for wind energy potential assessment relying on Weibull parameters estimation." *Wind* 2, no. 4 (2022): 617-635.
23. Karaboga, Dervis, and Bahriye Akay. "A comparative study of artificial bee colony algorithm." *Applied mathematics and computation* 214, no. 1 (2009): 108-132.
24. Singh, Shakti, and Subhash Chandra Kaushik. "Optimal sizing of grid integrated hybrid PV-biomass energy system using artificial bee colony algorithm." *IET Renewable Power Generation* 10, no. 5 (2016): 642-650.
25. Singh, Nirbhow Jap, J. S. Dhillon, and D. P. Kothari. "Synergic predator-prey optimization for economic thermal power dispatch problem." *Applied Soft Computing* 43 (2016): 298-311.
26. Pradhan C, Senapati MK, Malla SG, Nayak PK, Gjengedal T. Coordinated power management and control of standalone PV-hybrid system with modified IWO-based MPPT. IEEE Systems Journal. 2020 Sep 14;15(3):3585-96.
27. Senapati MK, Pradhan C, Samantaray SR, Nayak PK. Improved power management control strategy for renewable energy-based DC micro-grid with energy storage integration. IET generation, transmission & distribution. 2019 Mar;13(6):838-49.
28. Senapati MK, Pradhan C, Calay RK. A computational intelligence based maximum power point tracking for photovoltaic power generation system with small-signal analysis. Optimal Control Applications and Methods. 2023 Mar;44(2):617-36.
29. Isa, Normazlina Mat, Chee Wei Tan, and A. H. M. Yatim. "A comprehensive review of cogeneration system in a microgrid: A perspective from architecture and operating system." Renewable and Sustainable Energy Reviews 81 (2018): 2236-2263.
30. Singh, Shakti, Prachi Chauhan, and Nirbhow Jap Singh. "Feasibility of grid-connected solar-wind hybrid system with electric vehicle charging station." Journal of Modern Power Systems and Clean Energy 9, no. 2 (2020): 295-306.
31. Yu, Huangjing, Heming Jia, Jianping Zhou, and Abdelazim Hussien. "Enhanced Aquila optimizer algorithm for global optimization and constrained engineering problems." Mathematical Biosciences and Engineering 19, no. 12 (2022): 14173-14211.
32. Oszust, Mariusz. "Enhanced marine predators algorithm with local escaping operator for global optimization." Knowledge-Based Systems 232 (2021): 107467.

33. Li, Cunbin, Xuefeng Jia, Ying Zhou, and Xiaopeng Li. "A microgrids energy management model based on multi-agent system using adaptive weight and chaotic search particle swarm optimization considering demand response." Journal of Cleaner Production 262 (2020): 121247.
34. Paliwal, Navin Kumar, Asheesh Kumar Singh, and Navneet Kumar Singh. "A day-ahead optimal energy scheduling in a remote microgrid alongwith battery storage system via global best guided ABC algorithm." Journal of Energy Storage 25 (2019): 100877.
35. Makhadmeh, Sharif Naser, Ammar Kamal Abasi, Mohammed Azmi Al-Betar, Mohammed A. Awadallah, Iyad Abu Doush, Zaid Abdi AlkareemAlyasseri, and Osama Ahmad Alomari. "A novel link-based multi-objective grey wolf optimizer for appliances energy scheduling problem." Cluster Computing 25, no. 6 (2022): 4355-4382.
36. Agushaka JO, Ezugwu AE, Abualigah L. Gazelle optimization algorithm: a novel nature-inspired metaheuristic optimizer. Neural Computing and Applications. 2023 Feb;35(5):4099-131.
37. Dehghani M, Montazeri Z, Bektemyssova G, Malik OP, Dhiman G, Ahmed AE. Kookaburra optimization algorithm: a new bio-inspired metaheuristic algorithm for solving optimization problems. Biomimetics. 2023 Oct 1; 8(6):470.
38. Lin, J., Yang, X., Niu, S., Yu, H., Zhong, J. and Jian, L., 2024. Inflatable Savonius wind turbine with rapid deployment and retrieval capability: Structure design and performance investigation. Energy Conversion and Management, 310, p.118480.
39. Priyanka Mishra, Jagdish Helonde, Mangesh Dindayal Nikose, A hybrid optimization approach for efficient power management in AC/DC microgrid configuration.2025 Nov. 110842.